Electronic Supplementary Material (ESI) for Journal of Materials Chemistry A.

Electronic Supplementary Material (ESI) for Journal of Materials Chemistry A.

Supporting Information

Heterostructures of Ni−Co−Al layered double hydroxide assembled on V_4C_3 MXene for high-energy hybrid supercapacitors

Xin Wang,[a,b] Hui Li,[a] Han Li,[a,b] Shuai Lin,[a*] Jin Bai,[a,b] Jianming Dai,[a] Changhao Liang,[a] Xuebin Zhu,[a*] Yuping Sun[a,c,d] and Shixue Dou[e]

[a] Key Laboratory of Materials Physics, Institute of Solid State Physics, Hefei Institute of Physical Science, Chinese Academy of Sciences, Hefei 230031, People's Republic of China

[b] University of Science and Technology of China, Hefei 230026, People's Republic of China

[c] High Magnetic Field Laboratory, Chinese Academy of Sciences, Hefei 230031, People's Republic of China

[d] Collaborative Innovation Center of Advanced Microstructures, Nanjing University, Nanjing 210093, People's Republic of China

[e] Institute for Superconducting and Electronic Materials, University of Wollongong, NSW 2500, Australia

***Corresponding author E-mail:** linshuai17@issp.ac.cn and xbzhu@issp.ac.cn

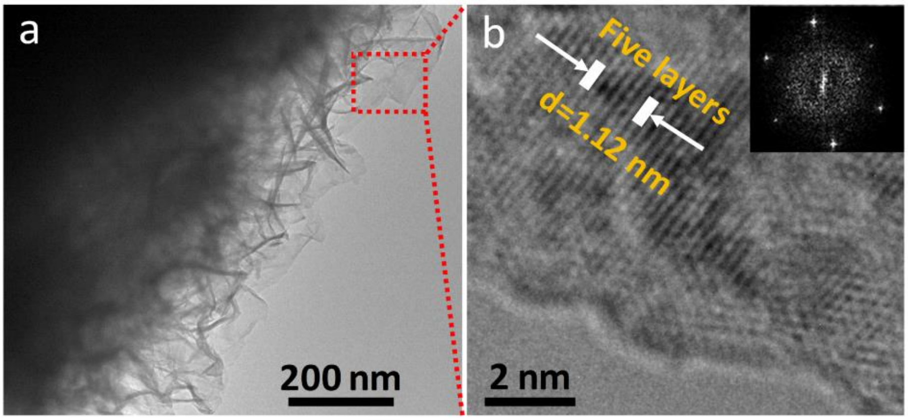

Figure S1 TEM image (a), HRTEM image (b) and Fast Fourier transform (FFT) in the inset of the NiCoAl-LDH/$V_4C_3T_x$.

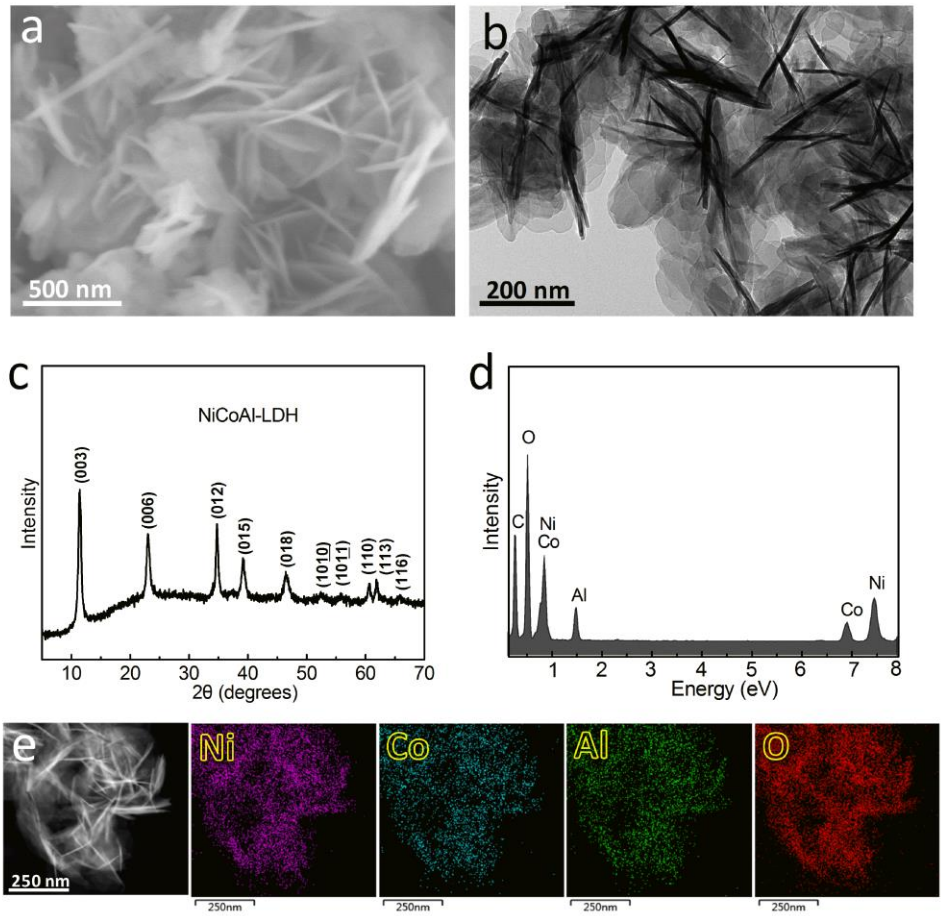

Figure S2. Characterizations of NiCoAl-LDH nanosheets. (a) FESEM image, (b)TEM image, (c) XRD pattern, (d) EDS spectra and (e) TEM image and corresponding elemental mapping images of Ni, Co, Al and O elements of NiCoAl-LDH nanosheets.

As shown in Figure S1c, the XRD pattern of NiCoAl-LDH illustrates that the diffraction peak can be assigned to a typical LDH with a rhombohedral microstructure.[1] Strong characteristic diffraction peaks of (003), (006) and (012) are clearly shown in Figure S1c, corresponding to the nickel-cobalt carbonate hydroxide hydrate.[2] Moreover, the sharp diffraction peaks strongly indicated that the as-prepared Ni-Co-Al-LDH was well crystallized. Figure S1a, b show the NiCoAl-LDH microstructures with the typical nanosheet structure. The elemental mapping images of NiCoAl-LDH indicate that the Ni, Co, Al and O elements have a relatively uniform distribution in the NiCoAl-LDH nanosheets (Figure S1e). XRD pattern, FE-SEM images, TEM images, elemental mapping images and EDS spectra (Figure S1d) together confirm that NiCoAl-LDH nanosheets have been successfully synthesized.

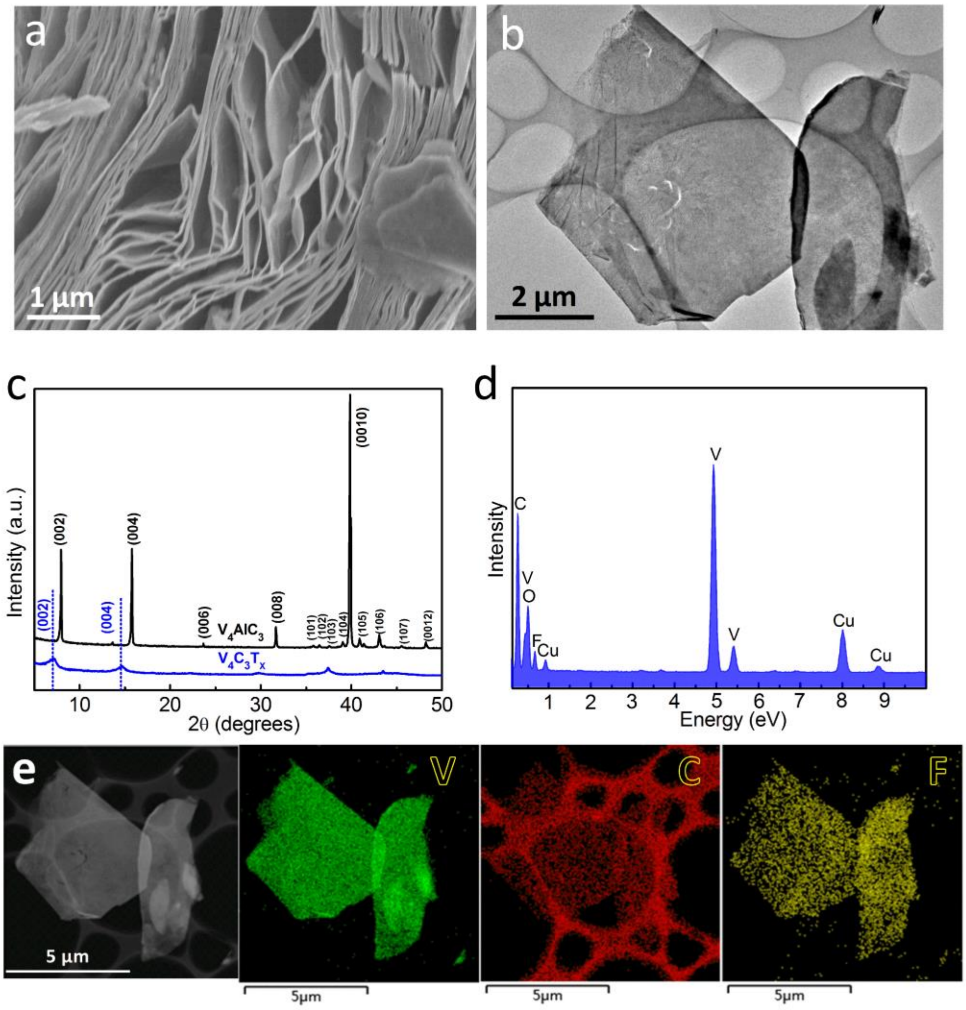

Figure S3. Characterizations of V_4C_3 MXene sheets. (a) FESEM image, (b)TEM image, (c) XRD pattern, (d) EDS spectra and (e) TEM image and corresponding elemental mapping images of V, C and F elements of V_4C_3 MXene sheets.

V_4AlC_3 powders were etched in hydrofluoric acid (HF) to synthesize $V_4C_3T_x$ MXene. XRD patterns for the as-prepared V_4AlC_3 bulk and V_4AlC_3 after HF treatment are shown in Figure S2c. It is observed that the (002) and (004) peaks of $V_4C_3T_x$ MXene appeared after 96 hours HF etching. The organ-like grain morphology of the HF etched V_4AlC_3 powder is shown in the FE-SEM image (Figure S2a), revealing the typical MXene morphology in accordance with previous reports.[3-8] The TEM image (Figure S2b) in Fig. 2d shows the typical MXene characteristics. The elemental mapping images of $V_4C_3T_x$ indicate that the V, C, O and F elements have a relatively uniform distribution in the $V_4C_3T_x$ sheets (Figure S2e). XRD pattern, FE-SEM images, TEM images, elemental mapping images and EDS spectra (Figure S2d) together confirm that $V_4C_3T_x$ MXene have been successfully synthesized.

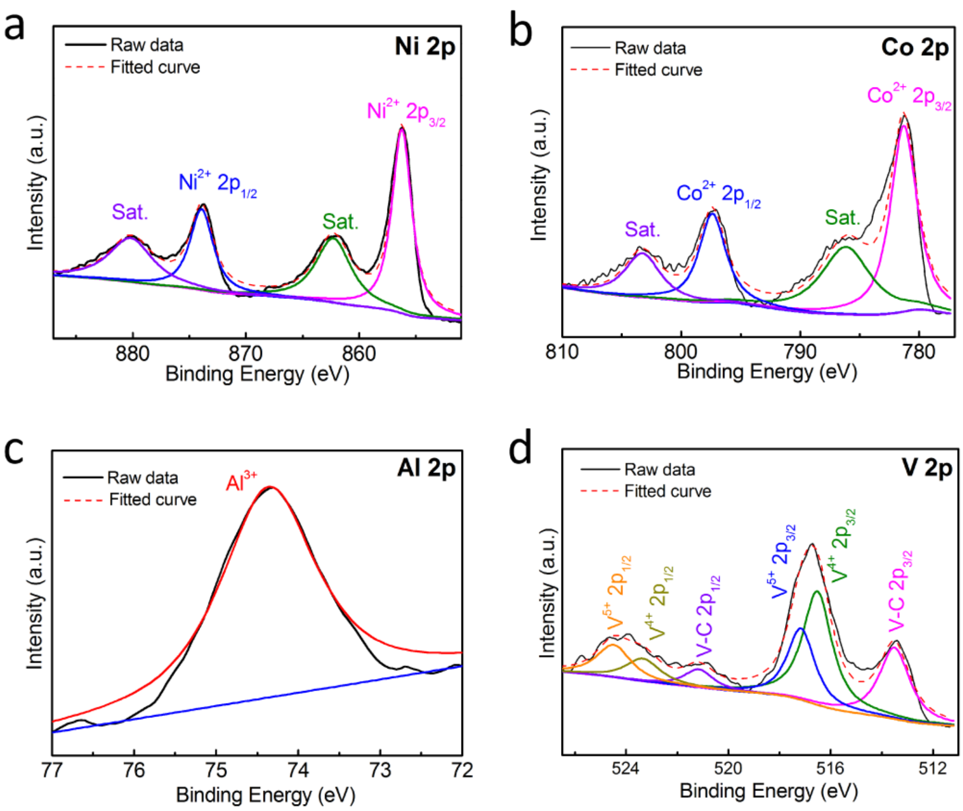

Figure S4. (a) Ni 2p, (b) Co 2p, (c) Al 2p and (d) V 2P XPS spectrum of NiCoAl-LDH/$V_4C_3T_x$

All XPS peaks were calibrated by C 1s. The Ni 2p spectrum (Figure S3a) has two major peaks Ni 2p1/2 around 874.0 and Ni 2p3/2 at 856.2 eV with a spin-energy separation of 17.8

eV and satellite peak at 880.3 and 862.3 eV, which indicates Ni^{2+}. Furthermore, a similar case can be found for Co 2p spectrum (Figure S3b), corresponding to Co^{2+}. The Al 2p peak (Figure S3c) is located at 74.3 eV, which indicates the Al^{3+} in NiCoAl-LDH/$V_4C_3T_x$ composite.[9, 10] As shown in Figure S3d, the binding energy of the V-C species, including V $2p_{3/2}$ (513.5 eV) and V $2p_{1/2}$ (521.1 eV) well match previous reports on vanadium carbides.[4, 11] The peaks at V $2p_{3/2}$ (517.2 eV) and V $2p_{1/2}$ (524.5 eV) can be attributed to V^{5+}, and the peaks at V $2p_{3/2}$ (516.6 eV) and V $2p_{1/2}$ (523.4 eV) are due to V^{4+}.

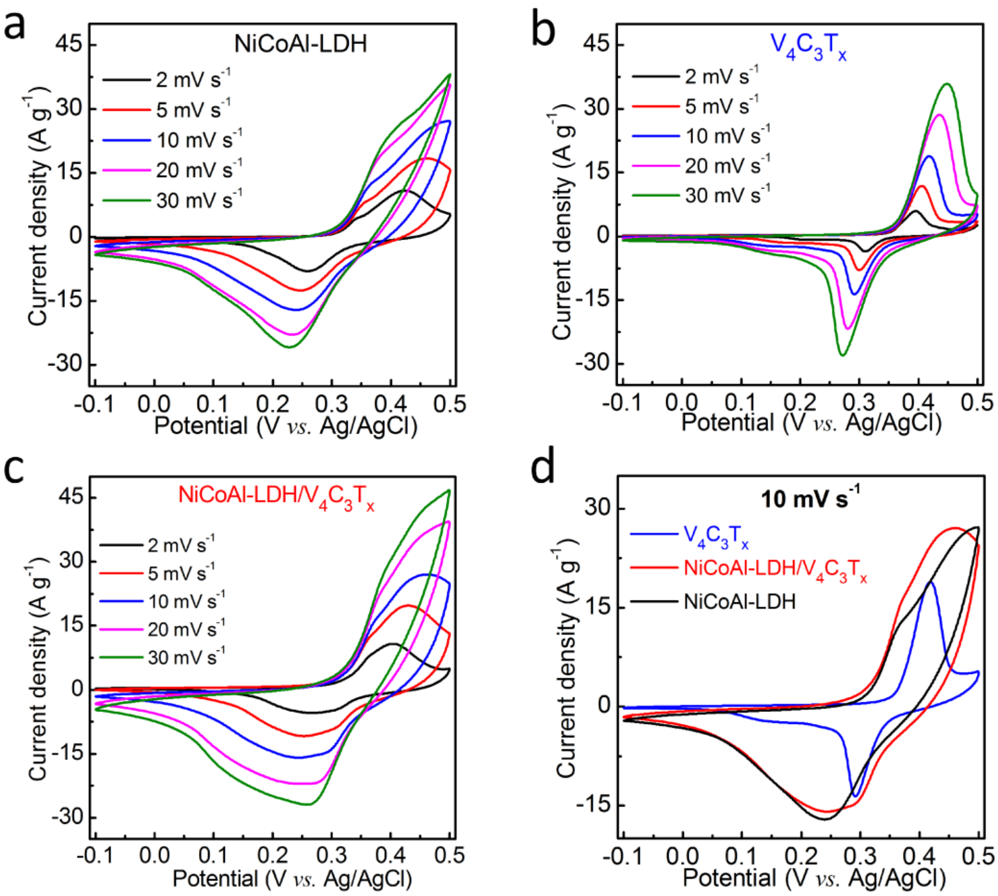

Figure S5. Cyclic voltammetry (CV) measurements of NiCoAl-LDH (a), $V_4C_3T_x$ (b) and NiCoAl-LDH/$V_4C_3T_x$ (c) electrodes at different scan rates, CV curves of NiCoAl-LDH, $V_4C_3T_x$ and NiCoAl-LDH/$V_4C_3T_x$ electrodes at a scan rate of 10 mV s^{-1}.

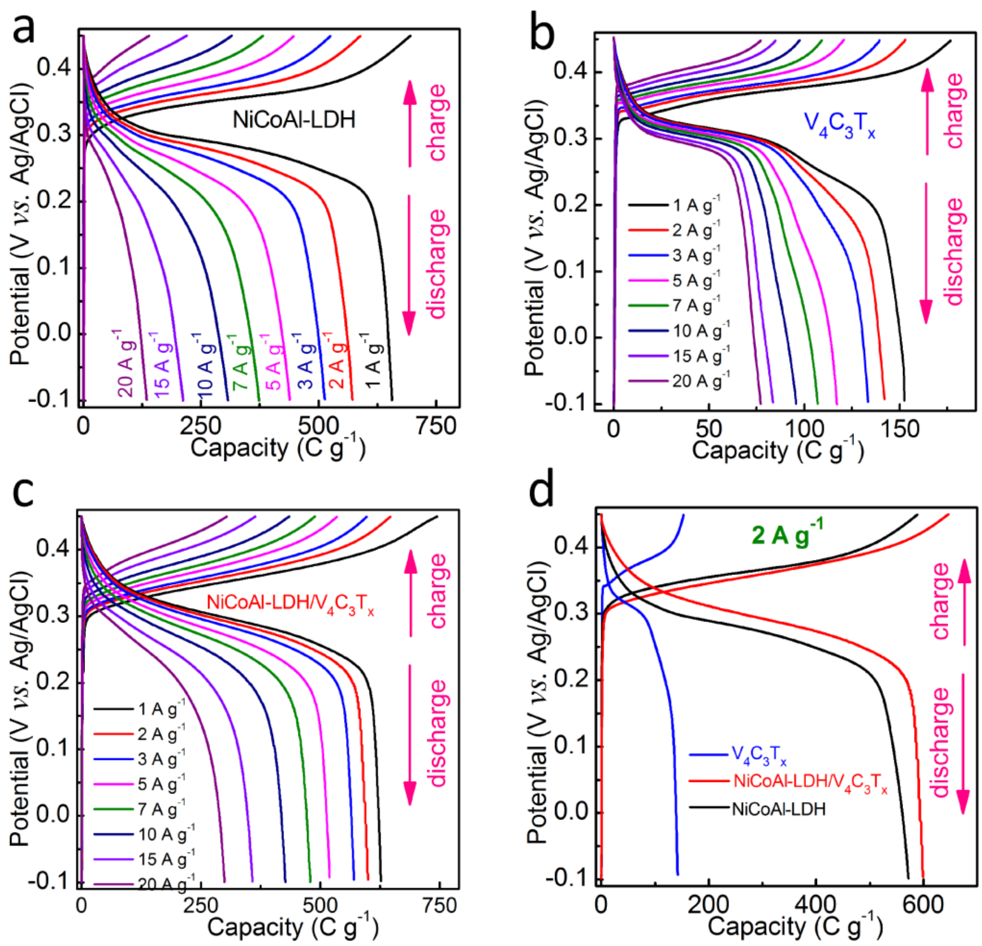

Figure S6. Galvanostatic charge-discharge(GCD) curves of NiCoAl-LDH (a), $V_4C_3T_x$ (b) and NiCoAl-LDH/$V_4C_3T_x$ (c) electrodes at different current densities, GCD curves of NiCoAl-LDH, $V_4C_3T_x$ and NiCoAl-LDH/$V_4C_3T_x$ electrodes at a current density of 2 A g^{-1}.

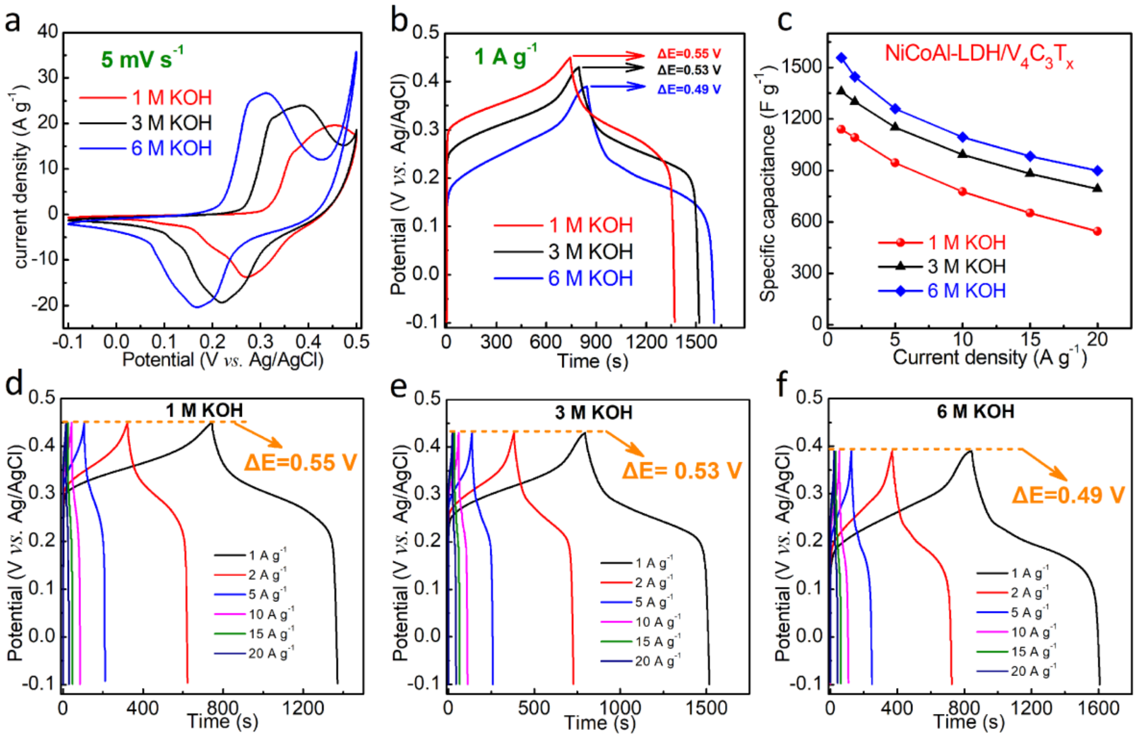

Figure S7. (a) CV curves at 5 mV s^{-1}, (b) galvanostatic charge-discharge (GCD) curves at 1 A g^{-1}, (c) the dependence of specific capacitance on the current densities of the NiCoAl-LDH/$V_4C_3T_x$ electrodes in 1 M, 3 M and 6 M KOH electrolytes. GCD curves of NiCoAl-LDH/$V_4C_3T_x$ electrodes at different current densities in 1 M (d), 3 M (e) and 6 M KOH (f) electrolytes.

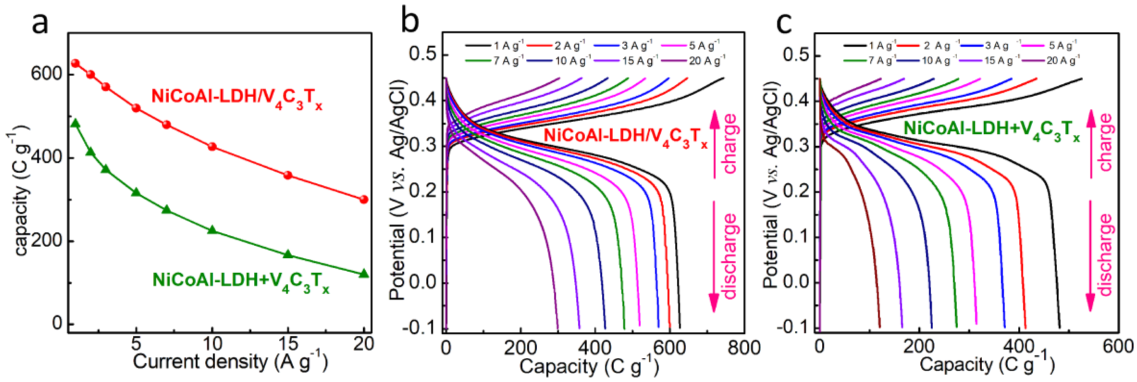

Figure S8. (a) Current density dependent specific capacitance for two different electrodes. Galvanostatic charge-discharge curves of NiCoAl-LDH/$V_4C_3T_x$ (b) and NiCoAl-LDH mixed $V_4C_3T_x$ (NiCoAl-LDH +$V_4C_3T_x$) (c) electrodes at different current densities in 1 M KOH electrolyte.

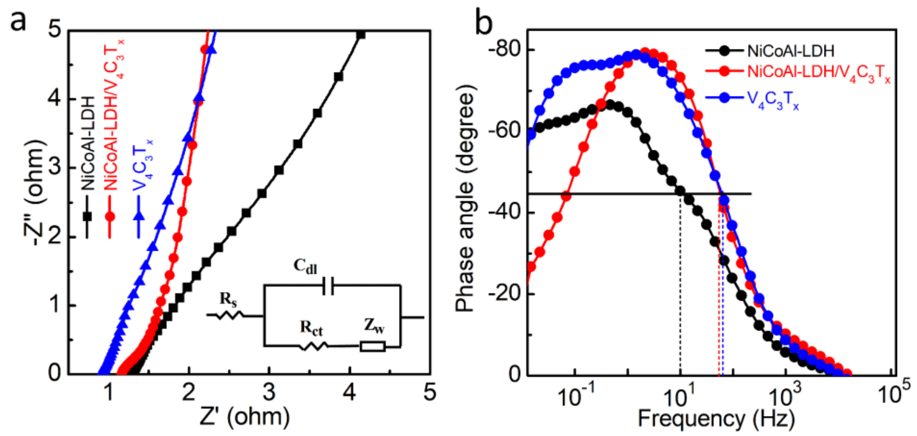

Figure S9. Comparisons of Nyquist plots and Bode plots of the NiCoAl-LDH and $V_4C_3T_x$, and NiCoAl-LDH/$V_4C_3T_x$ electrodes

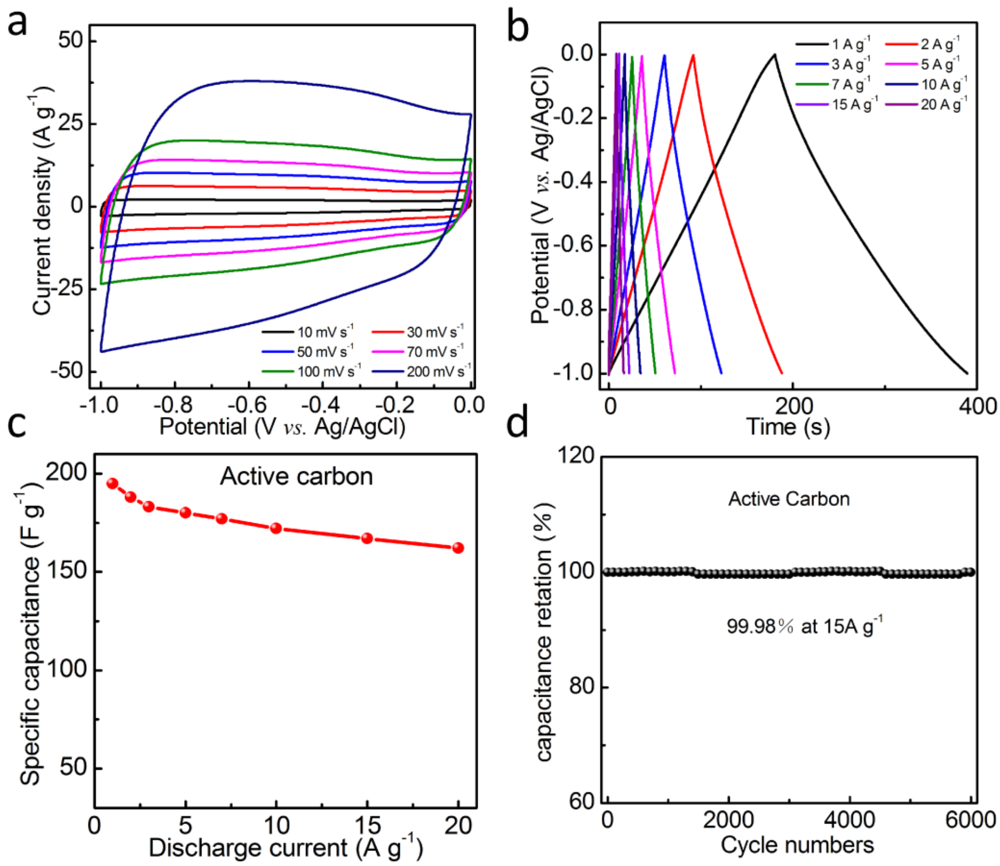

Figure S10. Electrochemical performance of activated carbon (AC) electrodes in 1 M KOH. (a) CV curves of the activated carbon (AC) electrodes at different scan rates. (b) Galvanostatic charge-discharge curves of the activated carbon (AC) electrodes at different current densities from 1-20 A g^{-1}. (c) Specific capacitances of the electrodes plotted as a function of discharge current density. (d) Cycling performance of activated carbon (AC) at 15 A g^{-1}.

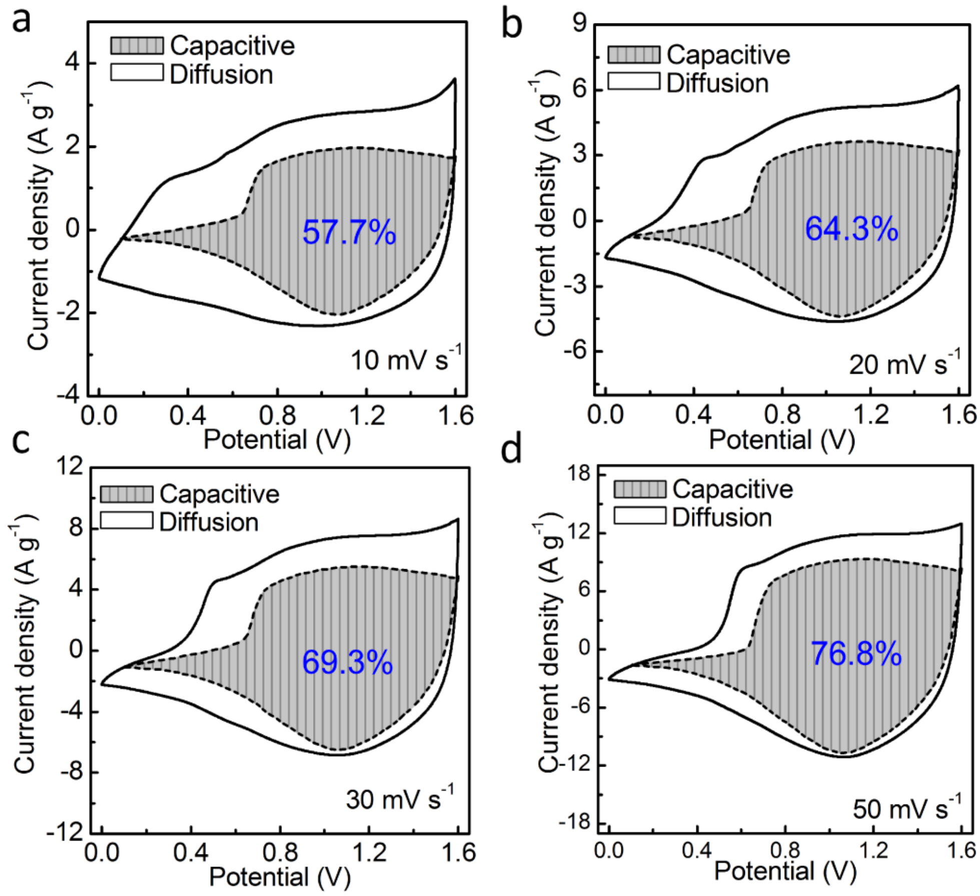

Figure S11. Kinetics and quantitative analysis of the NiCoAl-LDH/$V_4C_3T_x$//AC hybrid supercapacitor. Capacitive (gray) and diffusion-controlled (white) contribution to charge storage of NiCoAl-LDH/$V_4C_3T_x$//AC at 10, 20, 30, and 50 mV s^{-1}.

Table S1. The specific capacitance of NiCoAl-LDH/$V_4C_3T_x$ at 1, 2, 5, 10, 15 and 20 A g^{-1}.

NiCoAl-LDH/$V_4C_3T_x$	1A g^{-1}	2 A g^{-1}	5 A g^{-1}	10 A g^{-1}	15 A g^{-1}	20 A g^{-1}
1 M KOH	1140 F g^{-1}	1091 F g^{-1}	943 F g^{-1}	776 F g^{-1}	651 F g^{-1}	545 F g^{-1}
3 M KOH	1360 F g^{-1}	1300 F g^{-1}	1151 F g^{-1}	992 F g^{-1}	881 F g^{-1}	792 F g^{-1}
6 M KOH	1557 F g^{-1}	1445 F g^{-1}	1259 F g^{-1}	1094 F g^{-1}	984 F g^{-1}	898 F g^{-1}

Table S2. The specific capacity of $V_4C_3T_x$, NiCoAl-LDH/$V_4C_3T_x$, NiCoAl-LDH+$V_4C_3T_x$ and NiCoAl-LDH at 1, 2, 3, 5, 7, 10, 15 and 20 A g^{-1}.

Sample	1A g^{-1}	2 A g^{-1}	3 A g^{-1}	5 A g^{-1}	7 A g^{-1}	10 A g^{-1}	15 A g^{-1}	20 A g^{-1}
$V_4C_3T_x$	152 C g^{-1}	142 C g^{-1}	134 C g^{-1}	117 C g^{-1}	107 C g^{-1}	96 C g^{-1}	84 C g^{-1}	77 C g^{-1}
NiCoAl-LDH/$V_4C_3T_x$	627 C g^{-1}	600 C g^{-1}	570 C g^{-1}	519 C g^{-1}	479 C g^{-1}	427 C g^{-1}	358 C g^{-1}	300 C g^{-1}
NiCoAl-LDH+$V_4C_3T_x$	481 C g^{-1}	413 C g^{-1}	371 C g^{-1}	315 C g^{-1}	274 C g^{-1}	225 C g^{-1}	166 C g^{-1}	120 C g^{-1}
NiCoAl-LDH	656 C g^{-1}	571 C g^{-1}	512 C g^{-1}	438 C g^{-1}	373 C g^{-1}	307 C g^{-1}	211 C g^{-1}	134 C g^{-1}

Table S3. The Specific capacitance of active carbon (AC) at 1 A g^{-1}, 2 A g^{-1}, 3 A g^{-1}, 5 A g^{-1}, 7 A g^{-1}, 10 A g^{-1}, 15 A g^{-1} and 20 A g^{-1}.

Current density (A g^{-1})	1	2	3	5	7	10	15	20
Specific capacitance (F g^{-1})	195	188	183	180	177	172	167	162

Table S4. The specific capacitance of NiCoAl-LDH/$V_4C_3T_x$ //AC hybrid device at 1, 2, 3, 5, 7, 10, 15 and 20 A g^{-1}.

Current density (A g^{-1})	1	2	3	5	7	10	15	20
Specific capacitance (F g^{-1})	194	170	161	146	137	122	112	102

Table S5. Comparison of the cycling stability, energy and power density of the hybrid supercapacitors with those of advanced hybrid/asymmetric supercapacitors recently reported.

hybrid/asymmetric supercapacitors	Retention	Energy and power density	Refs.
NiCoAl-LDH/$V_4C_3T_x$//AC	98% after 10000 cycles at 20 A g^{-1}	71.7 Wh kg^{-1} at 830 W kg^{-1}; 45 Wh kg^{-1} at 20000 W kg^{-1}	This work
$NiCo_2S_4$ ball- in- ball hollow spheres//graphene/carbon spheres	78.6% after 10000 cycles at 5 A g^{-1}	42.3 Wh kg^{-1} at 476 W kg^{-1}	*Nat. Commun.* **2015**, 6,6694
$LiTi_2(PO_4)_3$//AC	85% after 1000 cycles at 10 mA cm^{-2}	24 Wh kg^{-1} at 200 W kg^{-1}; 15 Wh kg^{-1} at 1.0 kW kg^{-1}	*J. Power Sources* **2009**, 186, 224
PbO_2//AC	83% after 3000 cycles at 2.5 mA cm^{-2}	26.5 Wh kg^{-1} at 30.8 W kg^{-1}; 17.8 Wh kg^{-1} at 500 W kg^{-1}	*Electrochim. Acta* **2009**, 54, 3835
CoAl hydroxide/dodecyl sulfate anions/G//sandwiched G/porous C	84% after 2000 cycles at 100 mV s^{-1}	20.4 Wh kg^{-1} at 9.3 kW kg^{-1}	*Adv. Funct. Mater.* **2015**, 25, 1648
$NiMoO_4$//AC	14.3% after 10000 cycles at 5 A g^{-1}	60.9 Wh kg^{-1} at 850 W kg^{-1}; 41.1 Wh kg^{-1} at 17002 W kg^{-1}	*Adv. Energy Mater.* **2015**, 5
Fe_2O_3/functionalized G//MnO_2 /functionalized G	95% after 5,000 cycles at 0.5 A g^{-1}	50.7 Wh kg^{-1}at 100 W kg^{-1}	*Adv. Funct. Mater.* **2015**, 25, 627
AC//NiO-AC NFs	88% after 5000 cycles at 10 A g^{-1}	43.75 Wh kg^{-1} at 7.5 kW kg^{-1}	*J Mater Chem A* **2015**, 3, 7513
Ni-Co phosphate//AC solid-state device	90.5% after 5,000 cycles at 2 A g^{-1}	32.5 Wh kg^{-1} at 0.6 kW kg^{-1}	*Adv. Funct. Mater.* **2017**, 27
$CoMoO_4$-3D graphene//AC	87.42% after 10000 cycles at 1.67 A g^{-1}	21.1 Wh kg^{-1} at 300 W kg^{-1}; 3.59 Wh kg^{-1} at 6 kW kg^{-1}	*Adv. Mater.* **2014**, 26, 1044
NiO-porous C hollow sphere//N-doped G	86.4% after 10000 cycles at 6.7 A g^{-1}	50 Wh kg^{-1} at 740 W kg^{-1}; 26 Wh kg^{-1} at 14522 W kg^{-1}	*Energy Environ. Sci.* **2014**, 8, 188
$NaMnO_2$//AC	97% after 10 000 cycles at 10C	13.2 Wh kg^{-1} at 1.0 kW kg^{-1}	*J. Power Sources* **2009**, 194, 1222
CoO@ppy//AC	91.5% after 20 000 cycles at 25 mA cm^{-2}	43.5 Wh kg^{-1} at 87.5 kW kg^{-1}; 11.8 Wh kg^{-1} at 5.5 kW kg^{-1}	*Nano Lett.* **2013**, 13, 2078
Ni_3S_2/MWCNT-NC//AC	91% after 5000 cycles at 4 A g^{-1}	19.8 Wh kg^{-1} at 798 W kg^{-1}; 15.4 Wh kg^{-1} at 6.4 kW kg^{-1}	*ACS appl. Mater. & interfaces* **2013**, 5, 12168
C cloth@$NiCo_2O_4$ //C cloth@nitrogen-doped C flakes	86.7% after 20000 cycles of at 5 mA cm^{-2}	31.9 Wh kg^{-1} at 2.9 kW kg^{-1}; 27.3 Wh kg^{-1} at 22.9 kW kg^{-1}	*Adv. Energy Mater.* **2017**, 7, 1602391
$Na_4Mn_9O_{18}$//AC	84% after 4000 cycles at 0.5 A g^{-1}	34.8 Wh kg^{-1} at 62 W kg^{-1}; 21.0 Wh kg^{-1} at 337.4 W kg^{-1}	*J. Solid State Electrochem.* **2013**, 17, 1939
Ni-Co-Mn-OH/rGO//PPD/rGO	~91% after 10000 cycles at 20 A g^{-1}	74.7 W h kg^{-1} at 1.68 kW kg^{-1}	*Adv. Energy Mater.* **2018**, 8

Table S6. Energy density and corresponding power density of NiCoAl-LDH/$V_4C_3T_x$//AC hybrid supercapacitor.

Current density ($A\ g^{-1}$)	1	2	3	5	7	10	15	20
Energy density ($Wh\ kg^{-1}$)	71.7	68.1	65.4	61.1	57.4	52.5	48.3	45
Power density ($W\ kg^{-1}$)	830	803	2782	4741	6581	9692	14673	20000

References

1. Z. Liu, R. Ma, Y. Ebina, N. Iyi, k. Takada and T. Sasaki, *Langmuir*, 2007, **23**, 861-867.
2. Y. Dou, S. Zhang, T. Pan, S. Xu, A. Zhou, M. Pu, H. Yan, J. Han, M. Wei and D. G. Evans, *Adv. Funct. Mater.*, 2015, **25**, 2243–2249.
3. M. Naguib, M. Kurtoglu, V. Presser, J. Lu, J. J. Niu, M. Heon, L. Hultman, Y. Gogotsi and M. W. Barsoum, *Adv. Mater.*, 2011, **23**, 4248-4253.
4. M. Naguib, J. Halim, J. Lu, K. M. Cook, L. Hultman, Y. Gogotsi and M. W. Barsoum, *J. Am. Chem. Soc.* , 2013, **135**, 15966-15969.
5. M. R. Lukatskaya, S. Kota, Z. F. Lin, M. Q. Zhao, N. Shpigel, M. D. Levi, J. Halim, P. L. Taberna, M. Barsoum, P. Simon and Y. Gogotsi, *Nat. Energy*, 2017, **2**, 17105.
6. B. Anasori, M. R. Lukatskaya and Y. Gogotsi, *Nat. Rev. Mater.*, 2017, **2**, 16098.
7. B. Soundiraraju and B. K. George, *ACS Nano*, 2017, **11**, 8892-8900.
8. M. H. Tran, T. Schäfer, A. Shahraei, M. Dürrschnabel, L. Molina-Luna, U. I. Kramm and C. S. Birkel, *ACS Appl. Energy Mater.* , 2018, **1**, 3908-3914.
9. J. Yang, C. Yu, X. M. Fan, Z. Ling, J. S. Qiu and Y. Gogotsi, *J Mater Chem A*, 2013, **1**, 1963-1968.
10. J. Yang, C. Yu, X. M. Fan and J. S. Qiu, *Adv Energy Mater*, 2014, **4**, 1400761.
11. J. G. Choi, *Appl. Surf. Sci.*, 1999, **148**, 64-72.